

Demonstration of a superconducting diode-with-memory, operational at zero magnetic field with switchable nonreciprocity.

Taras Golod and Vladimir M. Krasnov*

Department of Physics, Stockholm University, AlbaNova University Center, SE-10691 Stockholm, Sweden.

Diode is one of basic electronic components. It has a nonreciprocal current response, associated with a broken space/time reversal symmetry. Here we demonstrate prototypes of superconducting diodes operational at zero magnetic field. They are based on conventional niobium planar Josephson junctions, in which space/time symmetry is broken by a combination of self-field effect from nonuniform bias and stray fields from a trapped Abrikosov vortex. We demonstrate that nonreciprocity of critical current in such diodes can reach an order of magnitude and rectification efficiency can exceed 70%. Furthermore, we can easily change the diode polarity and switch nonreciprocity on/off by changing bias configuration and by trapping/removing a vortex. This facilitates memory functionality. We argue that such diode-with-memory can be used for a future generation of in-memory superconducting computers.

I. INTRODUCTION

Large computation facilities, such as big data centers and supercomputers have become major energy consumers with a power budget often in excess of 100 MW. It has been argued that a small fraction of this power would be sufficient for cooling down the facility to cryogenic temperatures, suitable for operation of superconductors (SC) [1]. SC electronics would not only enable effective utilization of energy by removing resistive losses, it could also greatly enhance the operation speed. Since there is no resistance, $R = 0$, the RC time constant is no longer a limiting factor. The ultimate operation frequency is determined by the SC energy gap. For many SCs it is in the THz range [2]. This enables clock frequencies several orders of magnitude higher than for modern semiconducting electronics. Such perspectives have led to a renewed interest in development of a digital SC computer [1, 3–7].

Diode is one of the primary electronic components. Its nonreciprocal current-voltage (I - V) characteristics allows rectification of alternating currents, which is necessary for signal processing and ac-dc conversion. Diodes can be also used as building blocks for Boolean logics in digital computation. SC diodes should have strongly asymmetric critical currents, $|I_{c+}| \neq |I_{c-}|$. It is well known that nonreciprocity may appear in spatially asymmetric SC devices [8, 9]. SC diodes, based on spatially nonuniform Josephson junctions (JJs), were demonstrated long time ago [10]. Also SC ratchets [11], rectifying motion of either Josephson [12–15] or Abrikosov [16–23] vortices, were intensively studied. However, such spatially asymmetric devices operate only at finite magnetic fields, while computer components should work at zero field. Nonreciprocity at $H = 0$ is prohibited by the time-reversal symmetry, which requires invariance of electromagnetic characteristics upon simultaneous flipping of current and magnetic field [10, 24]. Therefore,

zero-field SC diode requires breaking of both space and time reversal symmetry.

Recently it was shown that nonreciprocity can be induced in noncentrosymmetric SC by spin-orbit interaction (SOI) [25–28]. This renewed search for diode effects in noncentrosymmetric SC [25, 28–30] and heterostructures [31–33]. SOI can induce asymmetry of either resistance in the fluctuation region near T_c [25–28, 30, 34], or supercurrent at low T [31, 32, 35–39]. However, SOI-based diodes require significant magnetic field. In several works zero-field SC diode operation was reported [33, 36], involving additional nontrivial effects. In this respect, nonreciprocity can be a tool for investigation of unconventional SC [34–39].

In this work we demonstrate prototypes of SC diodes with a large and switchable nonreciprocity of supercurrent at zero magnetic field. They are made of a conventional Nb SC and contain cross-like planar Josephson junctions with additional electrodes and an artificial vortex trap. Nonreciprocity is induced by a combination of self-field effect from asymmetric bias and stray fields from trapped Abrikosov vortex (AV). We demonstrate that the ratio, $|I_{c+}/I_{c-}|$, of such diodes can reach an order of magnitude and rectification efficiency can exceed 70%. Furthermore, we can switch nonreciprocity on and off, as well as change diode polarity in one and the same device. This is achieved by trapping/removing either a vortex, or an antivortex, and/or by changing bias configuration. This facilitates memory functionality. We argue that such diode-with-memory can be used for a new generation of superconducting in-memory computers.

II. THE CONCEPT

We consider the simplest case of a short JJ with the length $L < 4\lambda_J$, where λ_J is the Josephson penetration depth. This allows neglecting of complex phenomena associated with screening effects and Josephson vortices [9, 10, 40]. Realization of zero-field SC diode requires breaking of space/time symmetry. Time-reversal leads to

* Vladimir.Krasnov@fysik.su.se

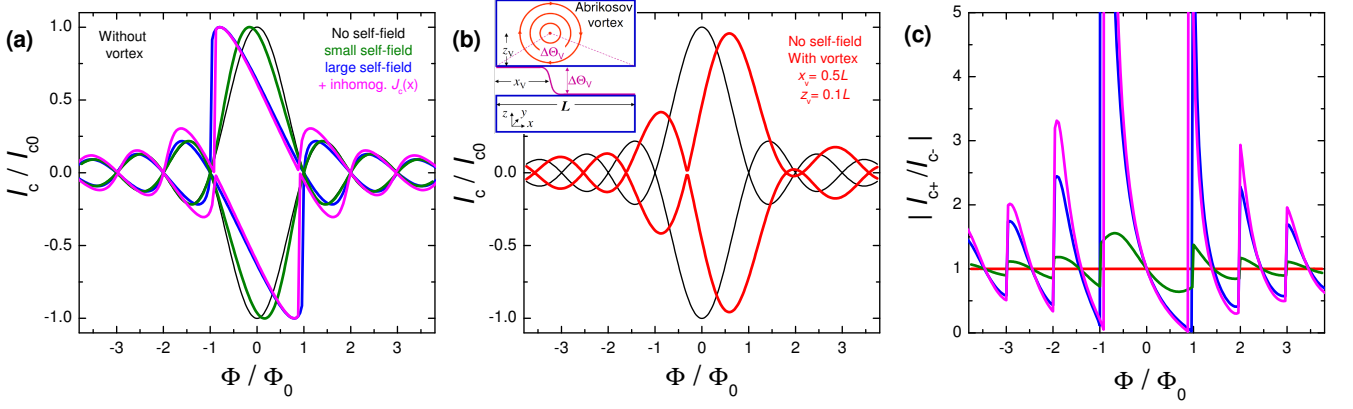


FIG. 1. **Numerical modelling of the two diode ingredients: (a) self-field induced by nonuniformity and (b) persistent stray fields from a trapped Abrikosov vortex.** (a) Simulated $I_c(\Phi)$ modulation: black - for a uniform JJ with constant critical current density, J_c , and bias, I_b ; olive - for $J_c = \text{const}$ with a slightly nonuniform bias, $I_b(x)$, leading to appearance of self-field; blue - for $J_c = \text{const}$ with a strongly nonuniform bias, $I_b(x)$; magenta - the same as for blue with added V-shape spatial inhomogeneity of $J_c(x)$. (b) Simulated $I_c(\Phi)$ for a uniform JJ with a uniform bias without (black) and with a trapped antivortex (red) at $x_v = L/2$ and $z_v = 0.1 L$. Inset shows a sketch of vortex-junction configuration. (c) Nonreciprocity, $|I_{c+}(\Phi)/I_{c-}(\Phi)|$, for the cases from (a) and (b) in the same color palette. It is seen that nonuniformity induces nonreciprocity, but only at a finite field, $H \propto \Phi \neq 0$. Vortex stray fields shift and distort $I_c(\Phi)$, but do not induce nonreciprocity.

inversion of transport currents and magnetic fields generated by these currents. The role of external field, H , is somewhat more tricky [24]. However, since it induces spatial phase gradient in a JJ, it is connected with the spatial symmetry [40].

Our concept has two simple ingredients: (i) Utilization of nonuniform bias for achieving nonreciprocity *at finite fields* [10]; and (ii) Shifting it to *zero field* by persistent stray fields from trapped AV [40–42]. These effects are summarized in Figs. 1 (a) and (b). Here black lines represent the conventional Fraunhofer modulation of the critical current versus magnetic flux, $I_c(\Phi)$, for a uniform JJ without a vortex. In this case there are both time-reversal, $I_{c+}(H) = |I_{c-}(H)|$, and space-reversal, $I_{c\pm}(H) = I_{c\pm}(-H)$, symmetries.

Nonuniformity of junction characteristics breaks spatial symmetry. Most common are nonuniform critical current density, $J_c(x)$, and bias current distribution, $I_b(x)$. Both lead to appearance of self-field effect [8–10]: nonuniformly distributed current generates magnetic field component parallel to H . Olive and blue lines in Fig. 1 (a) represent calculated $I_c(\Phi)$ patterns (see Methods) for small and large self-field effects in a JJ with nonuniform bias, $I_b(x) \neq \text{const}$, but uniform $J_c(x) = \text{const}$. Magenta lines are calculated for the same $I_b(x) \neq \text{const}$ as for the blue curves, with additional nonuniformity of $J_c(x) \neq \text{const}$. As discussed in Ref. [10], asymmetric nonuniformities of both $J_c(x)$ and $I_b(x)$ tilt $I_c(H)$ patterns and lead to appearance of nonreciprocity, $I_{c+}(H) \neq |I_{c-}(H)|$, at finite H . However, $I_c(H)$ remain centrosymmetric, $I_{c+}(H) = -I_{c-}(-H)$, for any nonuniformity. This is the consequence of space/time symmetry: simultaneous flipping of I and H is equivalent to looking at the same JJ from the back side and, therefore, should

lead to the identical observation [10].

Red lines in Fig. 1 (b) represent $I_c(\Phi)$ modulation in a uniform junction with a trapped AV, placed symmetrically in the middle of the electrode, $x_v = L/2$, at a distance $z_v = 0.1 L$ from the JJ, see the sketch in the inset. Stray fields from AV both distort and shift the $I_c(H)$ pattern [41–43]. This breaks space-reversal, $I_{c\pm}(H) \neq I_{c\pm}(-H)$, but preserves time-reversal, $I_{c+}(H) = |I_{c-}(H)|$, symmetry. Note that for short JJs this symmetry is preserved even for asymmetric vortex locations, $x_v \neq L/2$, but for long JJs all types of symmetries are removed due to appearance of Josephson vortices [40].

In Fig. 1 (c) we plot nonreciprocity, $|I_{c+}(\Phi)/I_{c-}(\Phi)|$, for the curves from panels (a) and (b). It is seen that uniform JJs without (black) or with (red) a vortex are reciprocal, $|I_{c+}/I_{c-}| = 1$. Nonuniform JJs exhibit nonreciprocity, which grows with increasing inhomogeneity of $J_c(x)$ and $I_b(x)$. Such Josephson diodes were studied earlier [10]. Their nonreciprocity could be very high: the largest peak at $\Phi/\Phi_0 \simeq -1$ for the magenta curve in Fig. 1 (c) reaches almost two orders of magnitude. However, due to centrosymmetric $I_c(H)$ there is no effect at $H = 0$.

For shifting nonreciprocity to $H = 0$, we utilize persistent stray fields from a trapped AV. As shown in Refs. [42, 43], flux offset introduced by AV in planar JJs is determined by the polar angle Θ_v of the vortex within the junction, see the sketch in Fig. 1 (b). It depends on the vortex location (x_v, z_v) , which is the tuning geometrical factor for the vortex-induced flux offset [42, 43]. In Figure 2 we show variation of $I_c(\Phi)$ modulation (left) and nonreciprocity, $|I_{c+}(\Phi)/I_{c-}(\Phi)|$, (right panels) upon approaching AV towards the junction from (a) $z_v = \infty$ to (e) $z_v = 0.01 L$ along the middle line $x_v = L/2$. Simu-

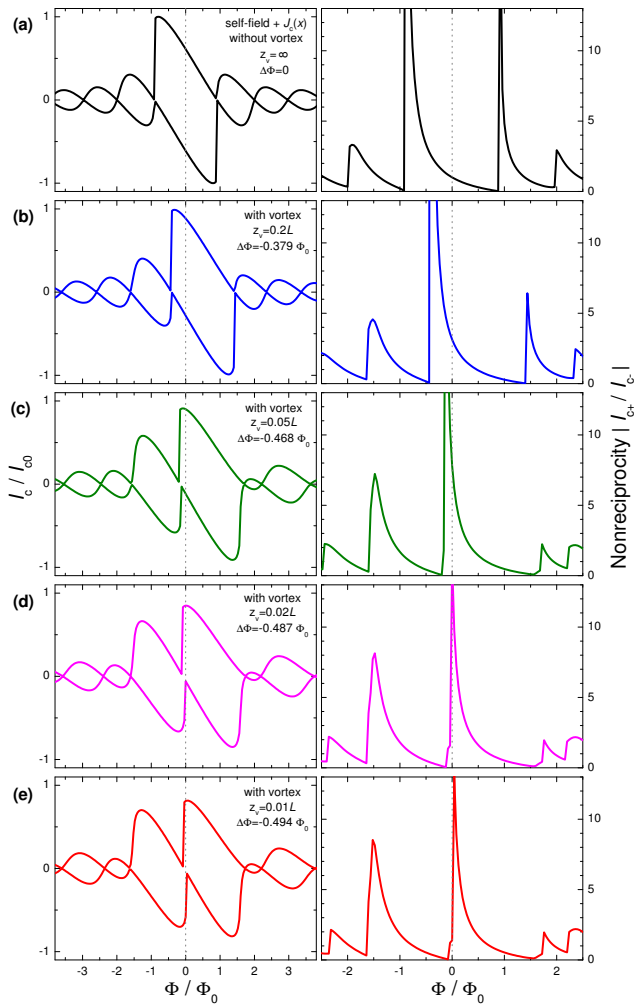


FIG. 2. **Numerical modelling of combined effects of nonuniformity and stray magnetic fields from a trapped vortex.** Left panels show simulated $I_c(H)$ patterns for a nonuniform JJ (the same as shown by magenta curves in Fig. 1) upon approaching an Abrikosov vortex along the middle line, $x_v = L/2$, from (a) $z_v = \infty$ to (e) $z_v = 0.01 L$. Right panels represent corresponding nonreciprocities, $|I_{c+}(H)/I_{c-}(H)|$. It is seen that upon approaching the vortex to the junction, growing stray fields progressively shifts nonreciprocal peaks. At a certain distance (d) the main peak passes through $H = 0$. This is the optimal geometrical configuration for a zero-field diode.

lations are done for the same nonuniform JJ depicted by the magenta line in Fig. 1. It is seen that with approaching the vortex to the JJ, the central nonreciprocal peak moves gradually from $\Phi/\Phi_0 \simeq -1$ towards 0 without significant reduction of the amplitude. At (d) $z_v = 0.05 L$ it passes through $\Phi = 0$. This is the optimal geometrical configuration for zero-field diode operation.

III. EXPERIMENTAL RESULTS

Figures 3 (a) and (b) show scanning electron microscope (SEM) images of two studied devices, D1 and D2. They have similar geometries. Each contains two planar JJs with $L = 5.6 \mu\text{m}$, seen as horizontal lines, and a vortex trap - a hole with diameter $\sim 50 \text{ nm}$, placed at $x_v \simeq L/2$ and $z_v \simeq 0.1 L$ from JJ1. D1 is made from a Nb(70 nm)/CuNi(50 nm) bilayer with superparamagnetic CuNi, while D2 is made from a single Nb film (70 nm). Therefore, D1 has proximity-coupled Nb-CuNi-Nb JJs and D2 contains variable thickness type constriction JJs, Nb-c-Nb. Both devices behave in a similar way, but Nb-c-Nb JJs have much larger $I_c R_n$, which can exceed 1 mV at low T [44]. This increases both the readout voltage and the upper operation frequency, $f_c = I_c R_n / \Phi_0$, which is advantageous for electronic applications. Details of junction fabrication, characterization and experimental setup can be found in Methods, Supplementary information [45] and Refs. [3, 41, 42, 44, 46–48]. Magnetic field is applied perpendicular to Nb film (in the y -direction).

As can be seen from Fig. 3 (b), studied devices have a cross-like geometry with four electrodes (left, right, top, bottom). This allows controllable introduction of asymmetric bias [47]. In Fig. 3 (c) we sketch three bias configurations for JJ1. Straight (bottom-to-top) bias does not generate H_y field component, while bias over right/left corners does induce positive/negative self-field H_y in the junction. This strongly affects junction characteristics and facilitates tunable introduction of spatial asymmetry.

Figs. 3 (d) and (e) show $I_c(H)$ patterns of JJ1 in the vortex-free case, measured using the three bias configurations for (d) D1 and (e) D2. Straight bias (olive curves) leads to regular Fraunhofer modulation. However, right (red) and left (blue) corner biases tilt $I_c(H)$ patterns in opposite directions due to appearance of self-fields [10]. Fig. 3 (f) shows the I - V characteristics at three fields indicated by dashed lines in Fig. 3 (d). At $H = 0$ (green) the I - V is symmetric $I_{c+} = |I_{c-}|$, however, at $H \simeq \pm 0.8 \text{ Oe}$, profound nonreciprocities appear, reaching an order of magnitude of either sign. This demonstrates that the cross-like geometry allows simple and controllable introduction of spatial (bias) asymmetry and associated nonreciprocity at $H \neq 0$.

Fig. 4 summarizes diode performance for D1 with the right-corner bias (a) without AV, and (b) with a trapped vortex, or (c) antivortex. AV is controllably introduced and removed by short current pulses [3, 43], as described in the Supplementary [45]. Top panels show $I_c(H)$ modulations for JJ1 (black) and JJ2 (olive). Red lines represent numerical fits (see Methods). In Fig. 4 (a) it is identical with the magenta curve in Fig. 1 (a). Fits in panels (b) and (c) are made for the actual geometry of the vortex trap and with AV-induced flux $\delta\Phi/\Phi_0 = \pm 0.47$ as a fitting parameter. It is consistent with $\Theta_{v1}/2\pi \simeq 0.44$ for JJ1 [45].

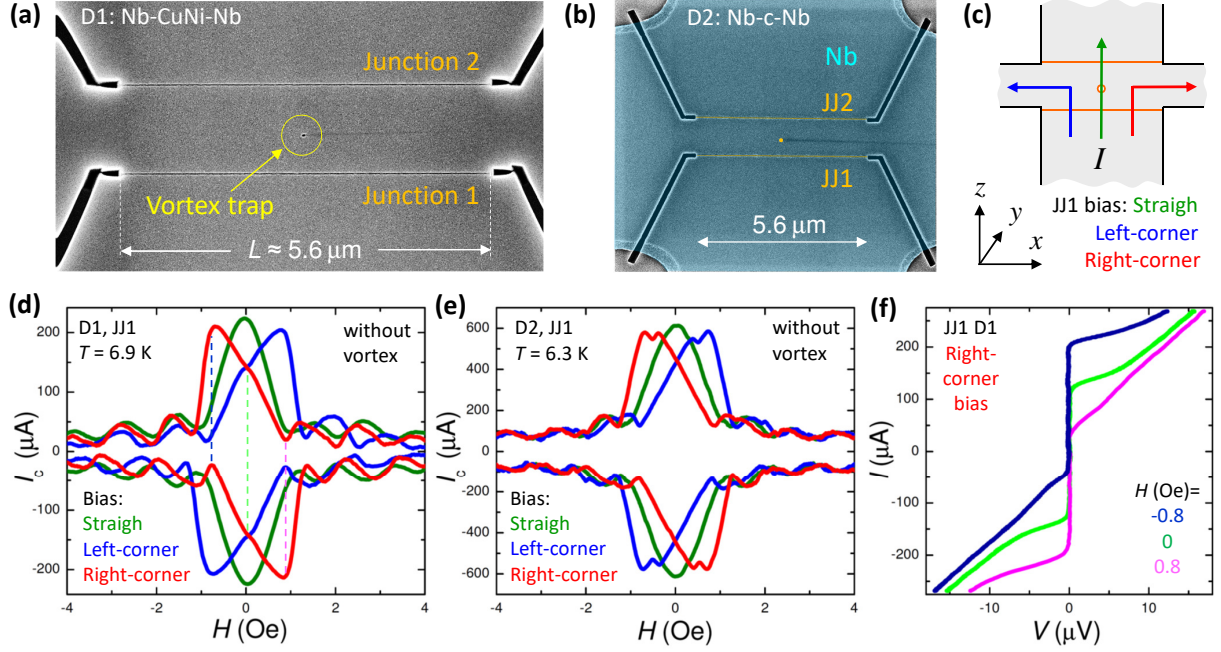


FIG. 3. **Device characterisation in the vortex-free case.** (a) and (b) SEM images of two studied devices: (a) D1 with Nb-CuNi-Nb junctions and (b) D2 with constriction-like Nb-c-Nb variable thickness bridges (false color). They have similar geometries and contain two planar junctions and a vortex trap. As seen from (b), devices have cross-like geometry with four electrodes (top, bottom, left, right). This allows controllable variation of self-field effect by changing bias configurations, as sketched in (c). Field is applied perpendicular to the film, in the y -direction, (x, y, z) is the right-handed coordinate system. (d) and (e) Measured $I_c(H)$ patterns for junctions 1 on (d) D1 and (e) D2 devices for three bias configurations. Straight bias (olive lines) does not induce self-field and leads to a regular Fraunhofer modulation without nonreciprocity. Left (blue) and right (red) corner bias induces self-fields of opposite signs, causing profound tilting of $I_c(H)$ patterns in opposite directions. (f) I - V curves for JJ1 on D1 at three magnetic fields marked by dashed lines in (d). A profound nonreciprocity with a factor ~ 10 difference between I_{c+} and $|I_{c-}|$ can be seen.

Middle panels in Fig. 4 represent main experimental results of this work: nonreciprocities $|I_{c+}/I_{c-}|$ and I_{c-}/I_{c+} for both JJs on D1. It can be seen that without AV, $|I_{c-}/I_{c+}|$ at $H \simeq 0.8$ Oe exceeds an order of magnitude, while it is absent at $H = 0$. Introduction of AV shifts the maxima so that a significant nonreciprocity occurs at zero field, as indicated by cyan ovals in (b) and (c). The maximum for JJ2 in (b) exceeds a factor four. For JJ1 it is slightly offset (by ~ 0.1 Oe) but still exceeds a factor two at $H = 0$. In (c) nonreciprocity at $H = 0$ is more than three for both JJs. Note, that diode polarity is opposite for vortex, $I_{c+} > |I_{c-}|$, and antivortex, $I_{c+} < |I_{c-}|$. Moreover, in our cross-like devices, the polarity can also be flipped by changing bias configuration. In Fig. 4 we use the right-corner bias. If we change to the left-corner bias, both self-field and polarity change sign, as demonstrated in Figs. 3 (d) and (e). For left-corner bias the polarity of vortex and antivortex states flips so that $|I_{c-}| > I_{c+}$ for vortex and $I_{c+} > |I_{c-}|$ for antivortex. All mentioned states are persistent and are achievable in one and the same device. Therefore, our diode is *switchable*. This enables memory functionality [3, 45] with three distinct states at $H = 0$: a reciprocal state “0” without AV, Fig. 4 (a), and states “+1” and

“-1” with positive and negative polarities, shown in Figs. 4 (b) and (c). Such reconfigurability is a unique property of vortex-based devices [43].

Rectification is an important property of a diode. Bottom panels in Fig. 4 show rectified time-average dc-voltage, calculated for ac-bias with the amplitude $I_{ac} = 220 \mu A$. Oscillatory field dependence with a significant rectified voltage at central peaks can be seen [10, 45]. The maximum rectifiable voltage for the case when one side of the I - V is fully open, $I_{ac} < I_c$, and the other is fully closed, $I_c = 0$, is $\langle V_{max} \rangle = I_{ac} R_n / \pi$. Central peaks for simulated red curves, which have nonreciprocities in the range of 30-50, are practically ideal. Experimental peaks for the vortex-free case (a) are exceeding 80 % of that value for the two central peaks. The peaks at $H = 0$ in (b) and (c) exceed 70 %, indicating good rectification efficiency of the diodes.

Figure 5 illustrates ac-bias dependence of rectification for D1 (a,b) and D2 (c,d). For clarity we consider the states with maximum nonreciprocity at finite H . The top panel in Fig. 5 (a) shows the I - V (royal) of JJ1 on D1 with near maximum $|I_{c+}/I_{c-}|$. Bottom panel shows time dependencies of voltage, for different ac-bias amplitudes. It is seen that for $|I_{c-}| < I_{ac} < I_{c+}$ only negative voltage

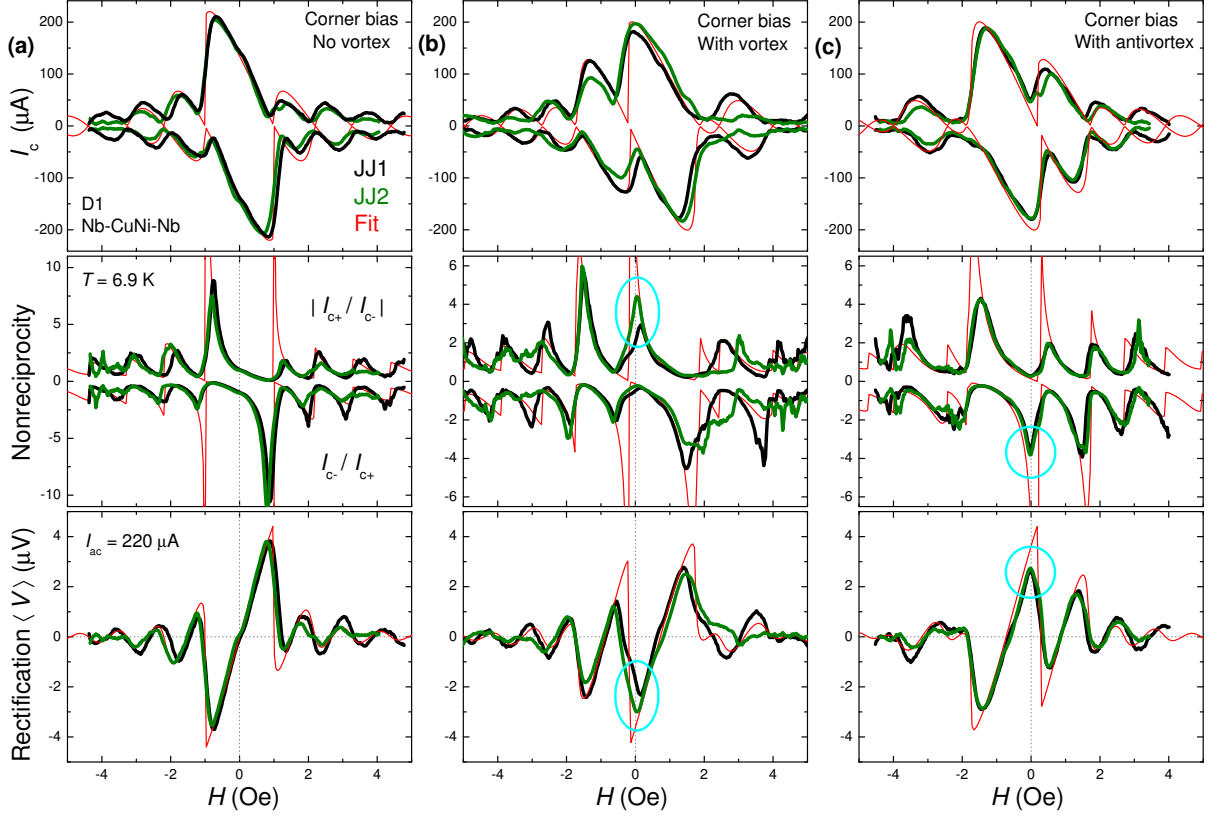


FIG. 4. **Diode operation with the right-corner bias.** (a) Without a vortex, (b) with a trapped vortex and (c) with an antivortex. Top panels show $I_c(H)$. Middle panels show nonreciprocities $|I_{c+}/I_{c-}|$, upper curves, and I_{c-}/I_{c+} , lower curves. Bottom panels show rectified dc-voltage calculated for harmonic ac-bias with $I_{ac} = 220 \mu\text{A} \simeq I_{c0}$. Black and olive lines represent data for junctions 1 and 2 on D1, red lines are numerical fits. Appearance of profound nonreciprocity and rectification at $H = 0$ is marked by cyan circles in (b) and (c). All measurements are performed at $T \simeq 6.9 \text{ K}$.

appears during the ac-oscillation period, leading to appearance of a negative time-average dc-voltage, $\langle V \rangle < 0$. Top panel in Fig. 5 (b) shows bias dependence of rectified voltage. It appears at $I_{ac} > |I_{c-}|$, grows linearly up to $I_{ac} = I_{c+}$ and then decreases due to progressive increase of positive voltages during the oscillation period, as seen from magenta and black $V(t)$ curves in Fig. 5 (a). The green line represents the ideal case with infinite nonreciprocity, $\langle V_{max} \rangle = I_{ac} R_n / \pi$. Bottom panel in Fig. 5 (b) shows rectification efficiency with respect to the ideal case, $\langle V \rangle / \langle V_{max} \rangle$. It is seen that the maximum efficiency, achieved at $I_{ac} = I_{c+}$, exceeds 80 %. The maximum rectification efficiency is close to $1 - 1/\nu$, where ν is the nonreciprocity of I_c .

Figs. 5 (c) and (d) demonstrate similar data for D2. Here we analyze the state, represented by the red I - V with maximum nonreciprocity of $|I_{c-}/I_{c+}|$. This leads to the opposite diode polarity, compared to Figs. 5 (a,c), with $\langle V \rangle > 0$. The overall performance is similar to D1, except for the larger $I_c R_n$ of Nb-c-Nb JJs, which results in proportionally larger rectified voltage and upper frequency range, $\sim I_c R_n / \Phi_0$ (see Supplementary [45] for additional clarifications).

To conclude, we demonstrated operation of a vortex-based Josephson diode with a large and switchable nonreciprocity at zero magnetic field. Our concept is based on utilization of nonuniform bias for inducing nonreciprocity and stray fields of Abrikosov vortex, trapped at a proper position, for shifting nonreciprocity to zero field. It is shown that such diodes have very good performance. Measured nonreciprocity of critical current exceeds a factor 4 at zero field and is more that an order of magnitude at finite field. Numerical modeling indicates that these values can be improved by another order of magnitude by careful design. The rectification efficiency exceeds 70 % at zero field. This is good enough for realization of more complex logical Boolean devices, needed for a digital superconducting computer. It has already been demonstrated [3] that a very simple geometry of such devices, which do not utilize SQUIDs, along with a nano-scale vortex size allows drastic miniaturization down to submicron dimensions. However, the most unique feature of our diodes is their switchability and tunability: (i) nonreciprocity at $H = 0$ can be easily introduced/removed by trapping/removing Abrikosov vortices using short current pulses and (ii) diode polar-

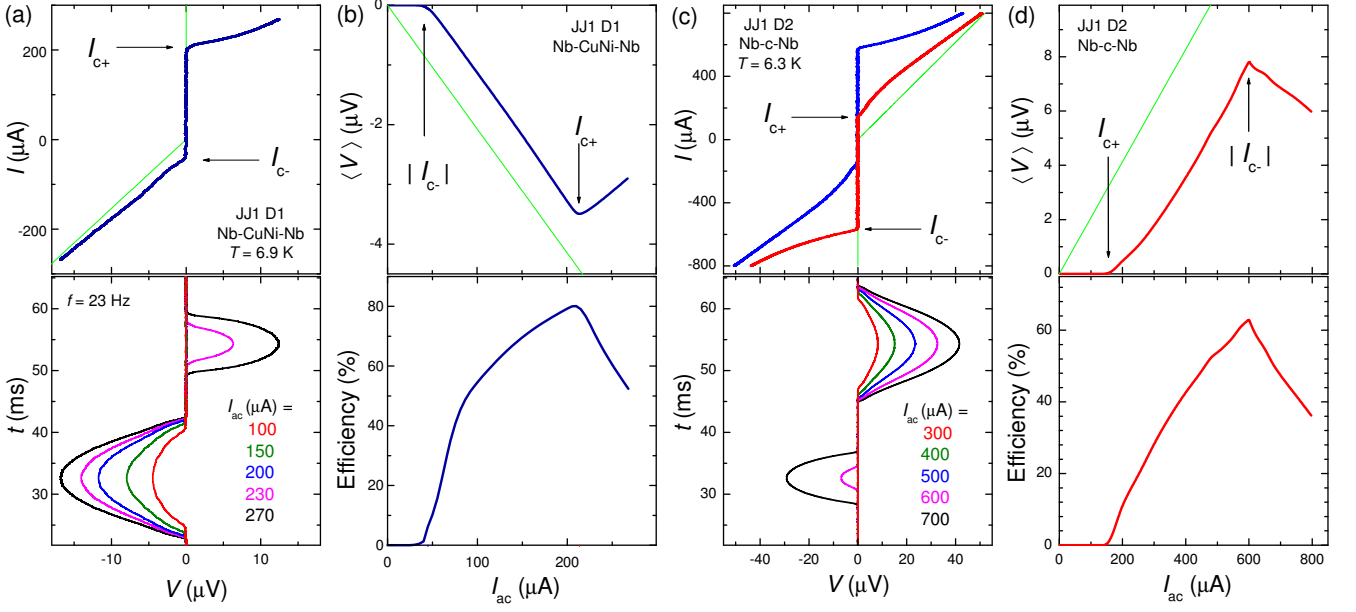


FIG. 5. **Amplitude dependence of rectification.** (a) Top: the I - V of JJ1 on D1 (dark blue) with nearly maximum nonreciprocity, $I_{c+}/|I_{c-}|$. It is measured using right-corner bias, $I = I_{ac} \sin(2\pi ft)$. Green line represents the ideal case with infinite nonreciprocity, $I_{c-} = 0$. Bottom: Time dependencies of voltages during one ac-period at $f = 23$ Hz for different bias amplitudes. (b) Top: time-averaged dc-voltage as a function of ac-bias amplitude for JJ1 on D1 at $T \simeq 6.9$ K. Green line represents the ideal case, $\langle V \rangle_{max} = I_{ac} R_n / \pi$. Bottom: rectification efficiency, $\langle V \rangle / \langle V \rangle_{max}$, versus ac-bias amplitude. (c) and (d) show similar data for JJ1 on D2 at $T = 6.3$ K. Top panel in (c) shows I - V s with maximum nonreciprocities obtained at $H = 0.7$ Oe (red) and -0.7 Oe (blue) without AV. (d) and bottom panel in (c) represent analysis of rectification for the red I - V with $I_{c+} < |I_{c-}|$, leading to a positive rectified voltage.

ity can be flipped by changing either the vortex sign, or the bias configuration. We argue that this may facilitate in-memory operation: an emerging new concept capable of boosting computer performance by avoiding bottlenecks associated with data shuffling between processor and memory [49]. This could open new perspectives for development of a digital superconducting computer. From this perspective it is advantageous that the diode is realized using conventional Nb-technology, which is mature enough for large-scale applications [6].

Methods

Samples.

Studied devices contain planar JJs. D1 is made from Nb (70 nm, top)/CuNi(50 nm, bottom) bilayer with superparamagnetic CuNi. D2 is made from a single Nb (70 nm) film. Films are deposited by dc-magnetron sputtering. They are first patterned into ~ 6 μm -wide bridges by photolithography and reactive ion etching, and subsequently nano-patterned by Ga^+ focused ion beam (FIB). Both Nb-CuNi-Nb (D1) and Nb-c-Nb (D2) JJs have a variable-thickness-bridge structure. They are made by cutting a narrow (20-30 nm) groove in the top Nb layer by FIB. Vortex trap (a hole ~ 50 nm in diameter) is also made by FIB. Both devices have similar cross-like geometry, as can be seen from Fig. 3 (b) and Supplementary Figure 1. They have practically identical dimensions, specified in details in the Supplementary [45]. We fabricated and tested similar JJs with other metals in the

bottom layer [3, 41, 42, 44, 46–48]. All of them work in a similar manner and results do not depend on the presence or specific material of the bottom layer.

Experimental details.

Measurements were performed in a closed-cycle cryostat. Magnetic field is applied perpendicular to the film (positive H along y -direction). $I_c(H)$ patterns were automatically recorded upon sweeping of magnetic field, provided by a superconducting solenoid. For this current-voltage characteristics were examined and I_c was determined using a small threshold voltage criterion, $V_{th} \sim 1 - 2$ μV . All I - V s shown in the manuscript are nonhysteretic.

Numerical simulations. Critical current is calculated by maximization of the Josephson current,

$$I_s = \int_0^L J_c(x) \sin[\varphi(x) + \varphi_0] dx, \quad (1)$$

with respect to the phase offset φ_0 . Here $J_c(x)$ is the critical current density along the JJ. The Josephson phase difference $\varphi(x)$ has two contributions [40]:

$$\varphi(x) = \frac{2\pi d_{eff}}{\Phi_0} B_y x + \varphi_v(x), \quad (2)$$

where d_{eff} is the magnetic thickness of the junction. Here the first term represents the linear phase gradient induced by the y -component of magnetic induction and

the second - a nonuniform phase shift induced by the trapped Abrikosov vortex. Since we consider only short junctions, we neglect possible screening effects and assume that B_y is uniform (x -independent). However, to account for the self-field effect we add an extra contribution to the applied external field H ,

$$B_y = H + L_{sf} I_s, \quad (3)$$

proportional to the total current and the self-field inductance, L_{sf} . The vortex contribution is given by the azimuthal angle [42], indicated in the sketch in Fig. 1 (b),

$$\varphi_v(x) = -V \arctan \left(\frac{x - x_v}{|z_v|} \right), \quad (4)$$

where V is the vorticity. Due to the self-field term in Eq. (3), I_s is present in the right-hand-side of Eq. (1) as well. This implicit equation is solved iteratively using the bisection method. The fitting is obtained by varying two constants: L_{sf} in Eq. (3) and V in Eq. (4); as well as allowing for a nonuniform $J_c(x)$ distribution in Eq. (1). The fit represented by magenta line in Fig.1 (a) and red lines in Fig. 4 corresponds to the V-shaped $J_c(x)$ with a 25% J_c reduction in the middle of the JJ, $x = L/2$.

-
- [1] D. S. Holmes, A.L. Ripple, and M.A. Manheimer, Energy-efficient superconducting computing - power budgets and requirements. *IEEE Trans. Appl. Supercond.* **23**, 1701610 (2013).
 - [2] E. A. Borodianskyi and V. M. Krasnov, Josephson emission with frequency span 1-11 THz from small $\text{Bi}_2\text{Sr}_2\text{CaCu}_2\text{O}_{8+\delta}$ mesa structures. *Nat. Commun.* **8**, 1742 (2017).
 - [3] T. Golod, A. Iovan, and V. M. Krasnov, Single Abrikosov vortices as quantized information bits. *Nature Commun.* **6**, 8628 (2015).
 - [4] I. I. Soloviev, N. V. Klenov, S. V. Bakurskiy, M. Y. Kupriyanov, A. L. Gudkov and A. S. Sidorenko, Beyond Moore's technologies: operation principles of a superconductor alternative. *Beilstein J Nanotechnol.* **8**, 2689 (2017).
 - [5] I. M. Dayton, T. Sage, E. C. Gingrich, M. G. Loving, T. F. Ambrose, N. P. Siwak, S. Keebaugh, C. Kirby, D. L. Miller, A. Y. Herr, Q. P. Herr, O. Naaman, Experimental demonstration of a Josephson magnetic memory cell with a programmable π -junction. *IEEE Magn. Lett.* **9**, 3301905 (2018).
 - [6] S. K. Tolpygo, V. Bolkhovsky, R. Rastogi, S. Zarr, A. L. Day, E. Golden, T. J. Weir, A. Wynn, and L. M. Johnson, Advanced Fabrication Processes for Superconductor Electronics: Current Status and New Developments. *IEEE Trans. Appl. Supercond.* **29**, 1102513 (2019).
 - [7] V. K. Semenov, Y. A. Polyakov, and S. K. Tolpygo, Very Large Scale Integration of Josephson-Junction-Based Superconductor Random Access Memories. *IEEE Trans. Appl. Supercond.* **29**, 1302809 (2019).
 - [8] S. A. Vasenko, K. K. Likharev, and V. K. Semenov, Static properties of distributed inhomogeneous Josephson junctions. *Zh. Eksp. Teor. Phys.* **81**, 1444-1455 (1981).
 - [9] A. Barone and C. Paterno, Physics and Applications of the Josephson Effect (J. Wiley & Sons, New York, USA, 1982).
 - [10] V. M. Krasnov, V. A. Oboznov, and N. F. Pedersen, Fluxon dynamics in long Josephson junctions in the presence of a temperature gradient or spatial nonuniformity. *Phys. Rev. B* **55**, 14486-14498 (1997).
 - [11] P. Hänggi and F. Marchesoni, Artificial Brownian motors: Controlling transport on the nanoscale. *Rev. Mod. Phys.* **81**, 387-442 (2009).
 - [12] F. Falo, P.J. Martinez, J. J. Mazo, T.P. Orlando, K. Segall, and E. Trias, Fluxon ratchet potential in superconducting circuits. *Appl. Phys. A* **75** 263-269 (2002).
 - [13] D.E. Shalom and H. Pastoriza, Vortex motion rectification in Josephson junction arrays with a ratchet potential. *Phys. Rev. Lett.* **94**, 177001 (2005).
 - [14] M. Beck, E. Goldobin, M. Neuhaus, M. Siegel, R. Kleiner and D. Koelle, High-efficiency deterministic Josephson vortex ratchet. *Phys. Rev. Lett.* **95**, 090603 (2005).
 - [15] H. B. Wang, et al., Fast Josephson vortex ratchet made of intrinsic Josephson junctions in $\text{Bi}_2\text{Sr}_2\text{CaCu}_2\text{O}_8$. *Phys. Rev. B* **80**, 224507 (2009).
 - [16] C.-S. Lee, B. Janko, I. Derenyi, and A.-L. Barabasi, Reducing vortex density in superconductors using the ratchet effect. *Nature* **400**, 337 (1999).
 - [17] J. E. Villegas, S. Savel'ev, F. Nori, E. M. Gonzalez, J. V. Anguita, R. Garcia, and J. L. Vicent, A Superconducting Reversible Rectifier That Controls the Motion of Magnetic Flux Quanta. *Science* **302**, 1188 (2003).
 - [18] Y. Togawa, K. Harada, T. Akashi, H. Kasai, T. Matsuda, F. Nori, A. Maeda, and A. Tonomura, Direct Observation of Rectified Motion of Vortices in a Niobium Superconductor. *Phys. Rev. Lett.* **95**, 087002 (2005).
 - [19] C.C. de Souza Silva, J. Van de Vondel, M. Morelle, and V. V. Moshchalkov, Controlled multiple reversals of a ratchet effect. *Nature* **440**, 651 (2006).
 - [20] S. A. Harrington, J.L. MacManus-Driscoll, and J.H. Durrell, Practical vortex diodes from pinning enhanced $\text{YBa}_2\text{Cu}_3\text{O}_{7-\delta}$. *Appl. Phys. Lett.* **95**, 022518 (2009).
 - [21] O.-A. Adami, D. Cerbu, D. Cabosart, M. Motta, J. Cuppens, W. A. Ortiz, V. V. Moshchalkov, B. Hackens, R. Delamare, J. Van de Vondel, and A. V. Silhanek, Current crowding effects in superconducting corner-shaped Al microstrips. *Appl. Phys. Lett.* **102**, 052603 (2013).
 - [22] J. Lustikova, Y. Shiomi, N. Yokoi, N. Kabeya, N. Kimura, K. Ienaga, S. Kaneko, S. Okuma, S. Takahashi, and E. Saitoh, Vortex rectenna powered by environmental fluctuations. *Nat. Commun.* **10**, 1038 (2018).
 - [23] Y.-Y. Lyu, J. Jiang, Y.-L. Wang, Z.-L. Xiao, S. Dong, Q.-H. Chen, M. V. Milosevic, H. Wang, R. Divan, J. E. Pearson, P. Wu, F. M. Peeters, and W.-K. Kwok, Superconducting diode effect via conformal-mapped nanoholes.

- Nat. Commun.* **12**, 2703 (2021).
- [24] D.Z. Albert, Time and chance. (Harvard University Press, Cambridge, MA, 2000).
 - [25] R. Wakatsuki, Y. Saito, S. Hoshino, Y.M. Itahashi, T. Ideue, M. Ezawa, Y. Iwasa, and N. Nagaosa, Nonreciprocal charge transport in noncentrosymmetric superconductors. *Sci. Adv.* **3**, e1602390 (2017).
 - [26] R. Wakatsuki and N. Nagaosa, Nonreciprocal Current in Noncentrosymmetric Rashba Superconductors. *Phys. Rev. Lett.* **121**, 026601 (2018).
 - [27] Y. Tokura and N. Nagaosa, Nonreciprocal responses from noncentrosymmetric quantum materials. *Nat. Commun.* **9**, 3740 (2018).
 - [28] F. Qin, W. Shi, T. Ideue, M. Yoshida, A. Zak, R. Tenne, T. Kikitsu, D. Inoue, D. Hashizume, and Y. Iwasa, Superconductivity in a chiral nanotube. *Nat. Commun.* **8**, 14465 (2017).
 - [29] J. Hu, C. Wu, and X. Dai, Proposed Design of a Josephson Diode. *Phys. Rev. Lett.* **99**, 067004 (2007).
 - [30] E. Zhang, X. Xu, Y.-C. Zou, L. Ai, X. Dong, C. Huang, P. Leng, S. Liu, Y. Zhang, Z. Jia, X. Peng, M. Zhao, Y. Yang, Z. Li, H. Guo, S.J. Haigh, N. Nagaosa, J. Shen, and F. Xiu, Nonreciprocal superconducting NbSe₂ antenna. *Nat. Commun.* **11**, 5634 (2020).
 - [31] F. Ando, Y. Miyasaka, T. Li, J. Ishizuka, T. Arakawa, Y. Shiota, T. Moriyama, Y. Yanase, and T. Ono, Observation of superconducting diode effect. *Nature* **584**, 373 (2020).
 - [32] C. Baumgartner, L. Fuchs, A. Costa, S. Reinhardt, S. Gronin, G. C. Gardner, T. Lindemann, M. J. Manfra, P. E. Faria Jr., D. Kochan, J. Fabian, N. Paradiso, and C. Strunk, Supercurrent rectification and magnetochiral effects in symmetric Josephson junctions. *Nat. Nanotechnol.* **17**, 39 (2022).
 - [33] H. Wu, Y. Wang, P. K. Sivakumar, C. Pasco, U. Filippozzi, S. S. P. Parkin, Y.-J. Zeng, T. McQueen, and M. N. Ali, The field-free Josephson diode in a van der Waals heterostructure. *Nature* **604**, 653 (2022).
 - [34] K. Yasuda, H. Yasuda, T. Liang, R. Yoshimi, A. Tsukazaki, K.S. Takahashi, N. Nagaosa, M. Kawasaki, and Y. Tokura, Nonreciprocal charge transport at topological insulator/superconductor interface. *Nat. Commun.* **10**, 2734 (2019).
 - [35] B. Pal, A. Chakraborty, P. K. Sivakumar, M. Davydova, A. K. Gopi, A. K. Pandeya, J. A. Krieger, Y. Zhang, M. Date, S. Ju, N. Yuan, N. B. M. Schröter, L. Fu, and S. S. P. Parkin, Josephson diode effect from Cooper pair momentum in a topological semimetal, *arXiv:2112.11285*.
 - [36] J.-X. Lin, P. Siriviboon, H. D. Scammell, S. Liu, D. Rhodes, K. Watanabe, T. Taniguchi, J. Hone, M. S. Scheurer, and J.I.A. Li, Zero-field superconducting diode effect in small-twist-angle trilayer graphene. *arXiv:2112.07841*.
 - [37] J. Diez-Merida, A. Diez-Carlon, S. Y. Yang, Y. M. Xie, X. J. Gao, K. Watanabe, T. Taniguchi, X. Lu, K. T. Law, and D. K. Efetov, Magnetic Josephson Junctions and Superconducting Diodes in Magic Angle Twisted Bilayer Graphene, *arXiv:2110.01067*.
 - [38] L. Bauriedl, C. Bäuml, L. Fuchs, C. Baumgartner, N. Paulik, J. M. Bauer, K.-Q. Lin, J. M. Lupton, T. Taniguchi, K. Watanabe, C. Strunk, and N. Paradiso, Supercurrent diode effect and magnetochiral anisotropy in few-layer NbSe₂ nanowires, *arXiv:2110.15752*.
 - [39] J. Shin, S. Son, J. Yun, G. Park, K. Zhang, Y. J. Shin, J.-G. Park, and D. Kim, Magnetic proximity-induced superconducting diode effect and infinite magnetoresistance in van der waals heterostructure, *arXiv:2111.05627*.
 - [40] V. M. Krasnov, Josephson junctions in a local inhomogeneous magnetic field, *Phys. Rev. B* **101**, 144507 (2020).
 - [41] T. Golod, A. Rydh, and V. M. Krasnov, Detection of the Phase Shift from a Single Abrikosov Vortex. *Phys. Rev. Lett.* **104**, 227003 (2010).
 - [42] T. Golod, A. Pagliero, and V. M. Krasnov, Two mechanisms of Josephson phase shift generation by an Abrikosov vortex. *Phys. Rev. B* **100**, 174511 (2019).
 - [43] T. Golod, R. A. Hovhannisyan, O. M. Kapran, V. V. Dremov, V. S. Stolyarov, and V. M. Krasnov, Reconfigurable Josephson Phase Shifter. *Nano Lett.* **21**, 5240 - 5246 (2021).
 - [44] S. Yu. Grebenchuk, R. Cattaneo, T. Golod, V. M. Krasnov, Nonlocal long-range synchronization of planar Josephson junction arrays. *arXiv:2201.11453*.
 - [45] See Supplementary information...
 - [46] V. M. Krasnov, O. Ericsson, S. Intiso, P. Delsing, V. A. Oboznov, A. S. Prokofiev, and V. V. Ryazanov, Planar S-F-S Josephson junctions made by focused ion beam etching. *Physica C* **418**, 16-22 (2005).
 - [47] T. Golod, O.M. Kapran, and V. M. Krasnov, Planar Superconductor-Ferromagnet-Superconductor Josephson Junctions as Scanning-Probe Sensors. *Phys. Rev. Appl.* **11**, 014062 (2019).
 - [48] A. A. Boris, A. Rydh, T. Golod, H. Motzkau, A. M. Klushin, and V. M. Krasnov, Evidence for Nonlocal Electrodynamics in Planar Josephson Junctions. *Phys. Rev. Lett.* **111**, 117002 (2013).
 - [49] H. Plattner and A. Zeier, In-Memory Data Management: Technology and Applications. (Springer Science & Business Media 2012), ISBN 9783642295744.